JOURNAL OF COMPUTATIONAL PHYSICS 33, 271–289 (1979)

A Finite-Circuit-Element Code for Modeling the Compression of a Gyrating Charged-Particle Beam

D. L. BOOK

Laboratory for Computational Physics, Naval Research Laboratory, Washington, D.C. 20375

P. J. TURCHI

Plasma Physics Division, Naval Research Laboratory, Washington, D. C. 20375

AND

D. L. STEIN

Joseph Henry Laboratory, Princeton University, Princeton, New Jersey 08540

Received August 2, 1978; revised February 20, 1979

A method is described for calculating the interaction between an imploding liner, a magnetically confined charged-particle ring (Astron e-layer, ion ring) and a target plasma, based on the equations of the equivalent circuit. Expressing the electrodynamical behavior in terms of inductive coupling between circular current loops, so that changes in geometry and plasma parameters are described by changes in the induction coefficients, means that only ordinary differential equations arise, in contrast with fluid descriptions. Induced electron currents are conveniently included in the model. Application to a beam–target fusion system driven by the compression of an ion ring is described as an illustration of the utility of the technique.

I. INTRODUCTION

Over the last several years a great deal of interest has arisen in connection with the topic of gyrating intense ion beams [1–3]. A ring or cylindrical current layer is produced by the motion of the ions in the superposed background (quasi-uniform) magnetic field and the poloidal self-field, with ring major radius R equal to the ion gyroradius. If the net current in such a configuration is strong enough, the direction of the field lines within the ring can be opposite that of the background field (Fig. 1). When the poloidal field on axis, $B_p = \mu_0 I/2R$, exceeds the background field B_0, the field in the interior region is completely reversed.

The system is assumed to be axisymmetric and to consist of fixed rigid conductors, deformable free conductors, and a ring composed of several species of charged particles. (The minor cross section of this ring need not be circular.) All these elements

0021-9991/79/110271-19$02.00/0

581/33/2-9

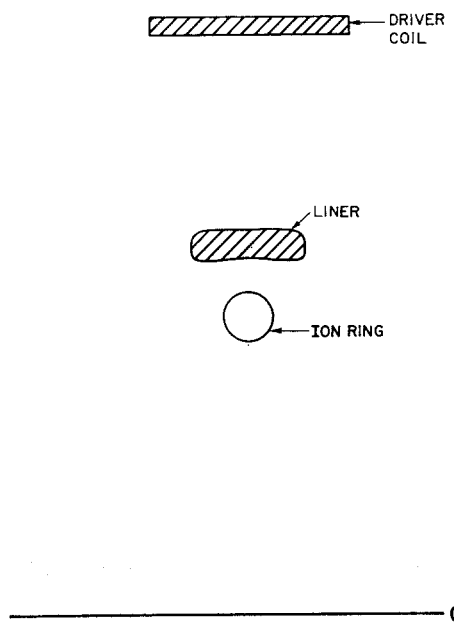

FIG. 1. Schematic of a fixed driver coil and moving liner and ion-beam plasma ring, all having finite length and roughly satisfying the large-aspect-ratio approximation.

carry current in the azimuthal direction and can have finite resistivity. They interact through $\mathbf{J} \times \mathbf{B}$ forces (that is, via Ampére's law). Displacement currents, hence all capacitances and effects propagating with speed c, are ignored. This is valid since the macroscopic motion of the currents is far too slow to produce significant electromagnetic radiation.

We drop the inertial terms from the particle equations of motion. Formally, the justification for this results from averaging the equations of motion for the jth particle species over a time long compared with the gyroperiod Ω_j^{-1} and short compared with the time scale for macroscopic motion, $\tau = R/\dot{R}$. The relative contribution from the inertial term left after this average is of order $(\Omega_j\tau)^{-1}$, typically much less than 10^{-3} for field strengths $\gtrsim 10$ T.

If a large number of current loops are used to represent the distribution of the current carried by the plasma and metal conductors in the system, this description is equivalent to a Lagrangian MHD code in $r-z$ coordinates. In most physical situations the dynamics of the plasma motion is of primary importance. However, for a certain class of problems, such as the transport and compression of charged-particle rings and imploding liner dynamics, the current-carrying elements move and deform markedly. These macroscopic motions are now the focus of our interest, and the details of the plasma processes become a distracting complication. Hence there is an advantage in seeking as simple as possible a representation of the plasma subsystem, even at the cost of some accuracy, provided the interaction between

plasma and metal conductors is well approximated. As will become clear, this reduces the problem to that of finding good approximations for the self- and mutual inductances associated with the various current loops.

Plasma collisions and transport are folded in by assuming a simple geometrical form (e.g., a thin e-layer, uniform-density proton ring, toroidal Bennett pinch, etc.) with a few time-dependent parameters in order to model self-consistent changes in the resistivity, transverse dimensions, loop forces, etc. A sufficient condition for such a model to succeed is that time scales associated with transport (e.g., thermal conduction time, particle diffusion time) be long compared with τ. This criterion is probably overly stringent, however, as such processes need not produce commensurate changes in the inductances.

The present paper describes a code developed for treating the dynamics of a gyrating ion ring interacting with a background plasma and a (possibly imploding) metal liner. The code is called IPICAC (for ion-beam-plasma interaction with cylindrical adiabatic compression). It is two dimensional (in r, z) and assumes axisymmetry, but does not employ finite differences on a two-dimensional grid to solve the dynamical problem. Instead, each portion of the system which carries current is regarded as part of a circular current loop. The beam is one such loop; the liner or wall may be approximated by several loops side by side. These current loops are coupled by their mutual inductances, and the dynamical behavior is determined through solution of the circuit equations. Thus the system is described by ordinary differential equations, rather than the partial differential equations of the usual magnetohydrodynamic treatment.

The principal difficulty in this approach lies in determining the inductances. These change as the geometry of the beam and liner changes, and have to be recalculated at every time step. Unless some approximation is invoked to simplify them, no computational advantage results from the circuit theory technique. Fortunately, such an approximation is available in many charged-particle ring configurations of interest, namely, that of large aspect ratio. That is, the major radius R_j of the jth current loop is taken to be large compared with its minor dimension and the separation in the r-z plane between it and any other loop. It is not necessary but is often convenient to assume that resistance and current are distributed uniformly throughout the r-z cross section of the loop. The latter may be of arbitrary shape, but is usually taken to be circular or rectangular.

In this conception, collisions between the ion beam and background plasma enter as a resistance (if more than one charge state is present, there can also be an Ohkawa current [4]). Plasma energy losses by radiation and convection also affect the beam dynamics through the inductances and the resistance. Consistent with this approach, the inertia of the various particle species is retained only in the centrifugal force, so that the beam and plasma remain in force balance with the wall currents.

The code described here was originally [1, 5] developed for an ion-beam–plasma interaction problem. We started with a ring of deuterium (D) ions, assuming an already existing field-reversed geometry. The ring was compressed by implosion of the liner, and the thermonuclear energy production arising from collisions between

the beam ions and T or He^3 target ions in the background plasma was studied. An attempt was made to balance the components of the system so that the collisional slowing-down of the beam ions just canceled their tendency to speed up because of angular-momentum conservation. "Clamping" the beam in this way at the energy for which the beam–target reaction rate peaks ($\sim$150 keV for D–T reactions) maximizes Q, the ratio of the yield to the sum of liner and plasma energy. It was found, however, that even with optimized parameters, Q was limited to 10% or less. The reason was that the energy given up by beam ions in collisions, most of which went into electron heating, caused expansion of the toroidal beam–plasma system in minor radius and reduced all of the number densities; and accordingly reduced the beam–target reaction rate. Presumably Q would increase if a method were found to cool the electrons and recycle their thermal energy.

Some results from this work will be displayed for purposes of illustration, but the method is much more general in applicability. Instead of assuming a preexisting state of field reversal, one can employ the code to study its origin and development in time. This problem will not, however, be addressed in the present paper, which is devoted to describing the code and some of the techniques employed in its implementation. The plan of the paper is as follows. In Section II we derive the equations of the circuit theory model of the beam–plasma–liner dynamical system. In Section III we discuss isentropic (lossless) compression of an ion ring and the role of the induced electron current in the resultant scaling. Collisions are described in Section IV. The implementation of conduction, particle transport processes, and other phenomena is discussed in Section V, and an example is described in Section VI. Our results are summarized in Section VII.

II. Liner Motion and Equivalent Circuit Equations

It is natural to represent the ion beam (and the currents carried by the electrons and target ion) as a current loop. It is equally convenient, though perhaps less natural, to represent the axial current profile on the liner (and possibly on the driver coil) as a superposition of coaxial current loops. Each such loop constitutes an electrical circuit individually coupled to each of the others, and contains a self-inductance and a resistance (arising from charged-particle encounters in the case of the ring). The circuit elements vary in time as the geometry changes.

Thus it is possible to calculate the implosion dynamics to any desired degree of realism entirely by means of the equivalent circuit equations. This representation is, in fact, a type of "finite-element" simulation. The minimum number of such circuits required to describe electromagnetic implosions of the liner is one each for the driver, liner and ring. In this limit the equivalent circuit is that shown in Fig. 2.

The circuit equations take the form

$$\frac{d\Phi_j}{dt} = -\mathscr{R}_j I_j \tag{1}$$

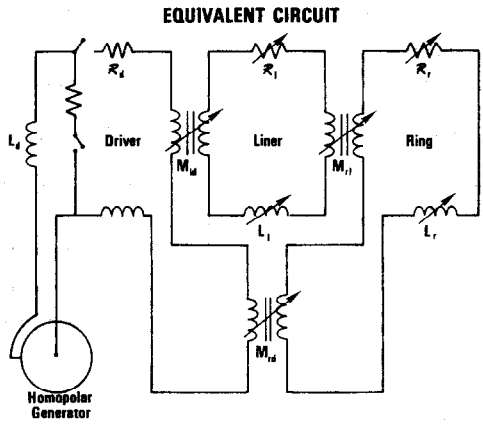

FIG. 2. Electrical circuit equivalent to Fig. 1. A homopolar generator is used to energize the driving coil.

where j runs over all current-carying loops in the system. For the circuit of Fig. 2, $j = d, l, r$ (signifying driver, liner, and ring, respectively). The flux threading the jth element is

$$\Phi_j = \sum_k \mathscr{M}_{jk} I_k , \tag{2}$$

where $\mathscr{M}_{jk}$ is the inductance coupling circuits j and k, and $\mathscr{R}_j$ is the resistance of the jth circuit. Equation (1) describes the evolution of Φ_j. Given a knowledge of the fluxes Φ_j and the induction coefficients $\mathscr{M}_{jk}$, Eq. (2) then can be solved for the I_j by matrix inversion.

If the driver is static and energized only during the outermost portion of the cycle we can make an additional simplification by restricting our attention to times when the liner and ring are far removed from the driver coil. Then j, k take on only the values l, r, and there are just two each of Eqs. (1) and (2). The numerical results described and plotted below were obtained using this two-loop circuit. It should be clear, however, that most of the discussion which follows is independent of the number of loops employed. We have experienced no difficulty in implementing versions of the code where as many as ten loops are employed to simulate the current profile in the liner. It appears that is would be easy to generalize the method to multiple ion rings or single rings with multiple constituent current filaments.

The coefficients $\mathscr{M}_{jk}$ are very easily calculated. Since the ring deforms freely, it tends to evolve so as to maximize its self-inductance, that is, toward a circular minor cross section. Moreover, one wants to consider configurations where ring and liner are close together, to minimize the volume filled with magnetic energy. Thus all distances separating current-carrying filaments are small compared with the major radii R, R_l (Fig. 1). In this limit the self- and mutual inductances can be calculated in the large-aspect-ratio approximation as

$$\mathscr{L}, \mathscr{M} \simeq \mu_0 R[\ln(8R) - 2 - \ln \bar{D}], \tag{3}$$

where the average is over the current-carrying part of the cross section, and the minor diameter D satisfies $D \ll R$.

Using (3) we find that the self-inductance of the ring is given by

$$\mathscr{L}_r \equiv \mathscr{M}_{rr} = \mu_0 R[\ln(8R/r) - 2 + \delta], \tag{4}$$

where r is the ring minor radius, and δ depends on the details of the assumed current profile. For example, if all the current is carried in a skin located at the minor radius, $\delta = 0$; if the current is uniformly distributed, $\delta = 0.25$; and if the ring looks like a Bennett pinch in cross section, $\delta = 0.5$. Similarly, the self-inductance of a liner segment is approximately (assuming the current is carried on the inner surface)

$$\mathscr{L}_l \equiv \mathscr{M}_{ll} \simeq \mu_0 R_l[\ln(8R/l) - \tfrac{1}{2}] \tag{5}$$

where l is the length of the segment, assumed much larger than the thickness, and R_l is the inside radius; and

$$\mathscr{M}_{lr} = \mu_0 (RR_l)^{1/2} \left\{ \ln \left[\frac{8(RR_l)^{1/2}}{[(R - R_l)^2 + (\frac{1}{2}l)^2]^{1/2}} \right] - 1 \right.$$
$$\left. - [(R_l - R)/(\tfrac{1}{2}l)] \tan^{-1}[(\tfrac{1}{2}l)/(R_l - R)] \right\}. \tag{6}$$

More important than the exact forms of (5) and (6) (which depend on the cross sections assumed to describe the liner) is the fundamental geometrical requirement $\mathscr{M}_{lr}^2 \leqslant \mathscr{L}_r \mathscr{L}_l$, with equality holding only if $R = R_l$. Since Eqs. (4)–(6) are approximate, this inequality must be enforced by means of an explicit interpolation; otherwise, the ring can pass right through the liner. The interpolation formula actually used is

$$\mathscr{M}_{lr} = \mathscr{M}_{lr} + [(\mathscr{L}_r \mathscr{L}_l)^{1/2} - \mathscr{M}_{lr}]\{1 + [(R_l - R)/r]^p\}, \tag{7}$$

where $\mathscr{M}$ is the corrected value of the mutual inductance. The dynamical results are not very sensitive to the choice of p, which was taken to be 10 in the numerical calculation.

As is well known from electromagnetic theory, the force tending to change any coordinate θ on which an inductive coefficient $\mathscr{M}_{jk}$ depends is given by

$$F_{jk} = -I_j I_k \frac{\partial \mathscr{M}_{jk}}{\partial \theta}. \tag{8}$$

Employing (8) consistently with the definitions used for $\mathscr{M}_{jk}$ guarantees conservation of total energy, the magnetic portion of which is

$$W_M = \tfrac{1}{2} \sum_{j,k} \mathscr{M}_{jk} I_j I_k = \tfrac{1}{2} \sum_j I_j \Phi_j. \tag{9}$$

Thus in carrying out numerical calculations, we determine the total force of the ring acting on the liner according to

$$F_l = -I_r \sum_j I_j \frac{\partial \mathscr{M}_{rj}}{\partial R_l}, \tag{10}$$

where the summation runs over the ring and all segments of the liner; the same expression with opposite sign yields the force with which the liner tends to hold the ring in place. The liner equation of motion is thus

$$M_l \ddot{R}_l = F_l , \tag{11}$$

where M_l is the liner mass.

Similarly, the electromagnetic force acting to constrict the ring is given by Eq. (8) with $\theta = r$:

$$F_r = -I_r \sum_j I_j \frac{\partial \mathscr{M}_{rj}}{\partial r} . \tag{12}$$

Most of the force F_r comes from the term containing $\mathscr{M}_{rr} \equiv \mathscr{L}_r$. Because of the use of the interpolation formula, Eq. (7), however, there is a small contribution from the liner–ring mutual inductance.

III. Isentropic Compression

It is possible to develop scaling laws in terms of which the liner motion and beam and plasma evolution are described by analytic expressions, provided we assume the absence of both fusion reactions and loss mechanisms. This model is not a useful starting point about which to perturb to describe a realistic reactor design, because the latter is quite sensitive to beam slowing and the heating resulting from production of charged fusion reaction products. It is, however, valuable in describing the dynamics in the absence of a target plasma, as well as guiding us in developing an intuition about the interdependence of various parts of the system.

If the liner is represented by J_l distinct current-carrying segments, there are $J_l + 1$ fluxes and $J_l + 11$ physical variables. In our numerical calculations we usually took $J_l = 1$. For this case the 12 physical quantities used to describe a dynamical state of the system are the fluxes Φ_l and Φ, linking the liner and ring, respectively; R and R_l; the ring minor radius r; the total numbers of beam and target ions, N_B and N_T, respectively; the beam, target, and electron temperatures, T_B, T_T, and T_e, respectively; and the mean azimuthal ion drift velocities v_B and v_T. To proceed, we write down all the conservation laws that are available. The conserved quantities are the magnetic flux threading the jth liner segment

$$\Phi_j = \sum_l \mathscr{M}_{jl} I_l + \mathscr{M}_{rj} = \Phi_j^0, \tag{13}$$

and that threading the ring,

$$\Phi_r = \mathscr{L}_r I_r + \sum_l \mathscr{M}_{rl} I_l = \Phi_r^0; \tag{14}$$

the specific angular momentum of beam ions,

$$Rv_B = R^0 v_B{}^0, \tag{15}$$

and of target ions,

$$Rv_T = R^0 v_T{}^0; \tag{16}$$

the total ion numbers for each species

$$N_B = N_B{}^0, \tag{17}$$

$$N_T = N_T{}^0; \tag{18}$$

and the beam, target, and electron entropy functions:

$$T_B V^{\gamma-1} = T_B{}^0 (V^0)^{\gamma-1}, \tag{19}$$

$$V_T V^{\gamma-1} = T_T{}^0 (V^0)^{\gamma-1}, \tag{20}$$

$$T_e V^{\gamma-1} = T_e{}^0 (V^0)^{\gamma-1}. \tag{21}$$

Here $V = 2\pi^2 R r^2$ is the volume of the beam/plasma ring. Superscripts (^{0}) indicate an initial or a reference state of the system (e.g., the state of maximum compression). To these equations must be added the condition of force balance on the ring in the direction of major and minor radius,

$$0 = I_r \sum_l I_l \frac{\partial \mathscr{M}_{rl}}{\partial R} + \frac{1}{2} I_r{}^2 \frac{\partial \mathscr{L}_r}{\partial R} + p \frac{\partial V}{\partial R} + \frac{N_B m_B v_B{}^2}{R} + \frac{N_T m_T v_T{}^2}{R} \tag{22}$$

and

$$0 = \frac{1}{2} I_r{}^2 \frac{\partial \mathscr{L}_r}{\partial r} + I_r \sum_l I_l \frac{\partial \mathscr{M}_{rl}}{\partial r} + p \frac{\partial V}{\partial r}, \tag{23}$$

respectively. Here $p = k(N_B T_B + N_T T_T + N_e T_e) V^{-1}$ is the internal pressure in the ring (k is the Boltzmann constant), and the electron number is obtained from the condition of charge neutrality,

$$N_e = N_B Z_B + N_T Z_T, \tag{24}$$

where Z_α is the charge state of ion species α. The last two terms in Eq. (22) are the centrifugal force terms derived from the circulation of the respective species; that corresponding to the target ions is usually negligible.

Equations (22) and (23) have been derived assuming that the ring inertia is negligible, i.e., that the ring repositions itself instantaneously in response to any change in the position of the liner. In addition, the electron mass has been set to zero systematically, as negligible in comparison with those of the ions. The ring current I_r satisfies

$$I_r = I_B + I_T + I_e, \tag{25}$$

where

$$I_B = \frac{N_B e Z_B v_B}{2\pi R}, \tag{26}$$

$$I_T = \frac{N_T e Z_T v_T}{2\pi R}, \tag{27}$$

and

$$I_e = -\frac{N_e e v_e}{2\pi R}. \tag{28}$$

Equations (1), (11), and (13)–(23) contribute a set of $12 + J_l$ fundamental algebraic equations in terms of the $12 + J_l$ physical quantities defining the state. [All the others are expressible in terms of these through Eqs. (2), (4)–(6), and (24)–(28).] Thus, specifying the state variables determines the evolution of the system completely. We rewrite the liner force equation as

$$\frac{d}{dt}(R_l\dot{R}_l) = \left\{R_l^2\dot{R}_l^2(R_l^{-2} - R_l'^{-2}) + \sum_l \left[\frac{1}{2} I_l^2 \frac{\partial \mathscr{L}_l}{\partial R_l} + I_l I_r \frac{\partial \mathscr{M}_{rl}}{\partial R_l}\right](2\rho L R_l)^{-1}\right\} \times [\ln(R_l'^2/R_l^2)]^{-1} \tag{29}$$

which parametrizes the dynamical history in terms of t. Equation (29) is derived by assuming conservation of the liner mass $M_l = 2\pi\rho L(R_l'^2 - R_l^2)$; ρ is the (uniform) liner density, L is the overall length, and R_l' is the outer liner radius.

Let us assume now that the electron current tending to neutralize I_B is zero. Then by conservation of angular momentum,

$$I_r = \frac{e}{2\pi R}(N_B v_B + N_T v_T) = \frac{e}{2\pi R^2}(N_B R v_B + N_T R v_T) \sim R^{-2}. \tag{30}$$

The minor radius force balance condition (23) reduces to

$$p = \frac{\mu_0}{4}\frac{R I_r^2}{V} \sim r^{-2}R^{-4}. \tag{31}$$

Equations (19)–(21), weighted by the respective total numbers N_j, sum to the adiabatic law

$$pV^\gamma = \text{const.} \tag{32}$$

Taking $\gamma = 5/3$ and combining (31) and (32) yields

$$r \sim R^{7/4}. \tag{33}$$

Hence the number densities for species α ($\alpha = B, T, e$), $n_\alpha = N_\alpha/V$, satisfy

$$n_\alpha \sim V^{-1} \sim R^{-9/2}, \tag{34}$$

and the poloidal field near the ring $B_p = \mu_0 I_r/2r$ satisfies

$$B_p^2 \sim p \sim R^{-15/2}. \tag{35}$$

We thus have a situation in which almost three-dimensional compression of the ring occurs as $R \simeq R_t$ is reduced. The poloidal field (35) rises almost as the inverse fourth power of R and the temperatures scale like $T \sim R^{-3}$.

At the other extreme, the motion of the liner may be such as to induce electron currents I_e totally neutralizing the change in ion current,

$$I_r \approx \text{const.} \tag{36}$$

Going through the same steps as above, we find

$$r \sim R^{-5/4} \tag{37}$$

and hence

$$n_\alpha \sim V^{-1} \sim R^{3/2} \tag{38}$$

and

$$B_p^2 \sim p \sim R^{5/2}. \tag{39}$$

In this limit the beam/plasma system *decompresses* during implosion, with n, p, and B_p decreasing.

The actual result obtained by numerical solution of the equations naturally lies between these two extremes. The ring is always observed to compress, but at a rate slower than that given by Eqs. (34) and (35), and the scaling is not a power law in R, If $I_e = 0$ initially, the behavior tends to resemble the second model increasingly as turnaround is approached. The dependence of the degree of field reversal on the magnitude of the electron current induced during compression [3] explains why attempts to derive a scaling law for this parameter [3, 6] do not appear to yield a simple result. There is, in fact, no clear-cut way to predict the scaling without specifying the geometry of the compression.

IV. Collisions

The electron thermal spread is assumed to be much larger than the thermal spread of either ion distribution or the relative drift between any two species. The average momentum transfer rate resulting from a collision between particles of species α and β is given by [9]

$$m_\alpha \left(\frac{dv_\alpha}{dt}\right)_\beta = -\nu_s^{\alpha/\beta} m_\alpha (v_\alpha - v_\beta), \tag{40}$$

where

$$\nu_s^{B/T} = \frac{4\pi Z_B^2 Z_T^2 e^4 (1 + m_B/m_T)\, n_T \ln \Lambda}{m_B^2 v_{BT}^3}; \tag{41}$$

$$\nu_s^{\alpha/e} = \frac{4(2\pi)^{1/2}}{3} \frac{Z_\alpha^2 e^4 (1 + m_\alpha/m_e)\, m_e^{3/2} n_e \ln \Lambda}{m_\alpha^2 (kT_e)^{3/2}}, \tag{42}$$

$\alpha = B, T$, and, from conservation of momentum,

$$n_\alpha m_\alpha \nu_s^{\alpha/\beta} = n_\beta m_\beta \nu_s^{\beta/\alpha}. \tag{43}$$

Here $\ln \Lambda$ is the form of the usual Coulomb logarithm appropriate to the species pair α, β, and $v_{\alpha\beta} = | v_\alpha - v_\beta |$. Correspondingly, the average temperature rate of change resulting from a collision is

$$k\left(\frac{dT_B}{dt}\right)_T = \frac{8\pi}{3}\frac{Z_B^2 Z_T^2 e^4}{m_B}\frac{n_T \ln \Lambda}{v_{BT}}, \tag{44}$$

$$k\left(\frac{dT_T}{dt}\right)_B = \frac{8\pi}{3}\frac{Z_B^2 Z_T^2 e^4}{m_T}\frac{n_B \ln \Lambda}{v_{BT}}, \tag{45}$$

for ion-ion encounters, and

$$k\left(\frac{dT_\alpha}{dt}\right)_e = \frac{8(2\pi)^{1/2}}{3}\frac{Z_\alpha^2 e^4 m_e^{1/2} n_e \ln \Lambda}{m_\alpha (kT_e)^{3/2}} k(T_e - T_\alpha), \tag{46}$$

$\alpha = B, T$, for ion-electron encounters, with the remaining rates $(dT_e/dt)_\alpha$ defined so as to satisfy conservation of energy.

Consideration of the magnitudes of these rate formulas reveals the following general features: (i) both electron and target ions contribute significantly to the rate at which beam ions slow down; (ii) the *relative* velocity with which beam ions move with respect to the target ions is chiefly affected by B–T collisions, because electron collisions act in the same sense (as a drag) on both ion species; (iii) thermalization of the beam also results principally from collisions with target ions.

On the basis of these generalizations, we can estimate the relative slowing down of beam and target ions through collisions as

$$\begin{aligned}\frac{d}{dt}(v_B - v_T)_{\text{coll}} &\simeq -(\nu_s^{B/T} - \nu_s^{T/B})(v_B - v_T) \\ &\equiv -\nu_s (v_B - v_T).\end{aligned} \tag{47}$$

For the usual case where the target ion mass density substantially exceeds that of the beam, $n_T m_T \gg n_B m_B$, Eq. (47) implies

$$\nu_s \simeq \nu_s^{B/T}. \tag{48}$$

At the same time, the adiabatic compression produced by the imploding liner tends to cause both ion species to accelerate in the azimuthal direction according to

$$\left(\frac{dv_\alpha}{dt}\right)_{\text{adiab}} = -v_\alpha \frac{\dot{R}}{R} \simeq -v_\alpha \frac{\dot{R}_l}{R_l} \tag{49}$$

Taking the difference between the beam and target equation (49) yields

$$\frac{d}{dt}(v_B - v_T)_{\text{adiab}} \simeq -\frac{\dot{R}_l}{R_l}(v_B - v_T). \tag{50}$$

Equations (47) and (50) give for the net time rate of change of the relative velocity

$$\frac{d}{dt}(v_B - v_T) \simeq -\left(\frac{\dot{R}_l}{R_l} + \nu_s\right)(v_B - v_T). \tag{51}$$

The condition that this relative velocity be a constant is thus

$$\dot{R}_l/R_l = -\nu_s\,. \tag{52}$$

When Eq. (52) is satisfied, the beam is said to be *clamped* [8]. With a tritium target there is an advantage in clamping the beam at a relative energy $\epsilon = \frac{1}{2}m_B v_{BT}^2 \sim 150$ keV which maximizes the reaction rate for D–T fusion.

Clamping is, of course, accompanied by a monotonic increase in thermal energy according to Eqs. (44) and 45). The ion thermal energy density $w_{\text{th}}^i = \frac{3}{2}k(n_B T_B + n_T T_T)$ increases as a result of ion–ion collisions at a rate

$$\begin{aligned}\frac{dw_{\text{th}}^i}{dt} &= \frac{4\pi Z_B^2 Z_T^2 e^4 n_B n_T \ln \Lambda}{v_{BT}}\left(\frac{1}{m_B} + \frac{1}{m_T}\right)\\ &= \nu_s^{B/T} n_B m_B v_{BT}^2\,.\end{aligned} \tag{53}$$

Using (48), we see by comparison of (52) and (53) that the time scale for implosions of the liner is comparable to that for heating up the ion beams. The electron heating rate can be even faster.

Note that if ν_s were approximately constant, the clamping condition (52) would imply an exponential decrease in R_l with time. As this is not realizable, clamping evidently cannot be maintained close to turnaround.

In differencing the equations in the code, we found it convenient to use as dependent variables quantities that are approximately conserved. Thus instead of T_α we used the entropy functions [Eqs. (19)–(21)], which now satisfy equations of the form

$$\frac{d}{dt}(T_\alpha V^{\gamma-1}) = V^{\gamma-1}\sum_\beta \nu_T^{\alpha/\beta}(T_\beta - T_\alpha), \tag{54}$$

where the $\nu_T^{\alpha/\beta}$ are defined as the rates in Eqs. (44)–(46). Similarly, the slowing-down rates enter as

$$\frac{d}{dt}(Rv_\alpha) = R\sum_\beta \nu_s^{\alpha/\beta}(v_\beta - v_\alpha). \tag{55}$$

V. Other Dissipative Processes

Collisions, discussed in Section IV, can transform directed energy into thermal energy. Although essential for clamping, they may be deleterious if they (i) increase the ratio of beam ion gyroradius to ring thickness excessively, (ii) cause too much of

the liner energy to go into pumping up the target plasma, or (iii) lead to premature loss of confinement as a result of decrease of beam current below that needed for field reversal. In addition, the following loss processes can remove energy from the system entirely: radiation, heat conduction along field lines, particle diffusion across lines, charge exchange with impurities, and Ohmic heating within the liner. The last of these can have a second, more serious consequence: finite resistivity gives rise to diffusion of field lines through the liner, untrapping the magnetic flux which holds the ring at a safe distance from the liner.

Radiation processes are modeled by adding loss terms to expression (55) for the time rate of change of the electron entropy function. For bremsstrahlung and synchrotron (cyclotron) radiation we have the terms

$$\frac{d}{dt}(V^{\gamma-1}T_e)_{\text{br}} = -V^{\gamma-1}[5.35 \times 10^{-24}(N_D + N_T Z_T^2)\, T_e^{1/2}] \tag{56}$$

and

$$\frac{d}{dt}(V^{\gamma-1}T_e)_{\text{cyc}} = -V^{\gamma-1}\left[3.98 \times 10^{-16}\frac{\beta^2 \bar{B}_p^{\,2}}{1-\beta^2}\right], \tag{57}$$

where T is given in eV, $\beta^2 = \frac{3}{2}kT_e/m_e c^2$ and $B_p = \mu_0 I_r/2r$. In the spirit of the circuit-theoretical approach (wherein the ring is a macroscopic circuit element with certain lumped parameters derived from microscopic processes), the radiation rates are calculated by averaging the field strength over the ring cross section.

In the same fashion, thermal conduction losses can be treated by writing

$$\frac{d}{dt}(V^{\gamma-1}T_\alpha)_{\text{cond}} = -V^{\gamma-1}4\pi^2 R r \kappa_\alpha \left(\frac{T_\alpha}{r}\right) = -V^{\gamma-1}4\pi R \kappa_\alpha T_\alpha\,, \tag{58}$$

where κ_α is the average cross-field thermal conduction of species α. (The fastest thermal loss process is that associated with the target ions, $\alpha = T$.) Furthermore, thermal equilibration, α-particle heating, etc., can be included in an average sense in the same form.

Finally, particle losses can be estimated simply by assuming smeared-out density profiles according to some law like the Bennett pinch. If a given profile extends past the position of the separatrix, located at average minor radius $r = r_s$, that portion of the particles located at $r > r_s$ is lost. A simple calculation then gives the loss rate as the rate at which particles "fall over the edge." Thus we find

$$\left(\frac{dN_\alpha}{dt}\right)_{\text{diff}} = -\frac{Gr^2}{r_s^{\,2}}\nu_s^{\,\alpha} N_\alpha\,, \tag{59}$$

where G is a geometrical factor (equal to 12 for a Bennett profile) which decreases as the assumed profile becomes more localized, and $\nu_s^{\,\alpha}$ is the total scattering rate for species α.

VI. A Numerical Example

The equations and solution techniques described in Sections II–V have been implemented in a computer code called IPICAC. The code advances the solution in time from one level to the next (at t and $t + \delta t$, respectively) by solving ordinary differential equations for the state variables, via the following sequence of steps:

(i) A Newton–Raphson routine is used to solve for r and R iteratively by requiring force balance in the charged-particle ring [Eqs. (22) and (23)]. At each iteration the derivatives with respect to r and R are found by means of difference approximations {i.e., $\partial F/\partial r \approx [F(r + \delta r, r) - F(r - \delta r, R)]/2\delta r$, etc.}

(ii) From knowledge of r and R, the inductive coefficients are found. Ion drift velocities are found from $v_j = (Rv)_j/R$, densities from $n_j = N_j/(2\pi^2 Rr^2)$, and electron drift velocity from Eqs. (24)–(28).

(iii) The force on the liner elements is calculated from Eq. (8).

(iv) From $T_j V^{\gamma-1}$ and $V = 2\pi^2 Rr^2$, T_j is calculated. T_j and v_j are used to obtain the effects of collisional resistivity on the linked magnetic flux and the drift velocities, and of thermal diffusion and equipartition on the temperatures.

(v) Radiation and particle-loss rates are found from Eqs. (56)–(59). Thermonuclear reaction rates, particle injection rates, etc., are computed, as appropriate.

(vi) The results of steps (ii)–(v) are used to calculate the time derivatives of all the dependent (state) variables. The time step δt is chosen sufficiently small that the iterative routine in (i) converges. (This is the most stringent condition and the only one in practice which must be observed.)

Initialization is carried out using the same equations, but solving them in a different order. The dimensions of the liner and ring are specified, along with the fluxes linking the liner and the ring, the beam energy, all particle temperatures, the poloidal field strength B_p, the fraction of current neutralization by electrons, and the relative concentration and drift velocities of the various ion species. These are sufficient to specify the state variables. The same quantities are dumped out at intervals and used to restart the calculation as required and are printed as diagnostics.

We consider the following situation. A liquid lithium liner (density $\rho = 0.54$ g/cm^3) of length $L = 13.5$ cm and inner and outer radii 31.59 cm and 48.43 cm, respectively, implodes with velocity 3×10^4 cm/s on a fully ionized D–He^3 ring with major and minor radii of 30 cm and 0.758 cm, respectively. The initial target ion number densities are $n_{He^3} = 2n_D = 3.59 \times 10^{16}$ cm^{-3}. The temperatures are $T_D = 23.7$ keV, $T_{He^3} = 1$ keV, and $T_e = 10$ keV. The deuterium current is 1.52 MA, twice the electron back current. These numbers are chosen to give a beam ion streaming energy of 550 keV and a poloidal field of 200 kG, with beam clamping. Since the emphasis was on determining Q, only the part of the evolution in the vicinity of liner turnaround was considered, and the early-time conditions giving rise to these parameters were not investigated.

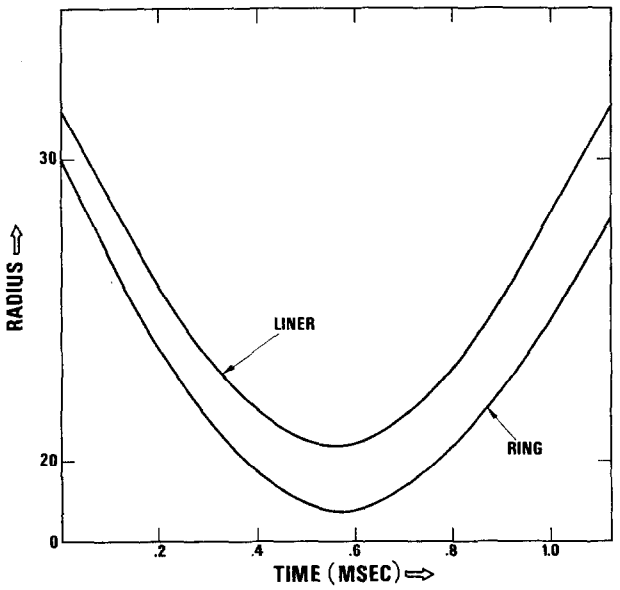

FIG. 3. Ring and liner radii versus t for the given initial conditions.

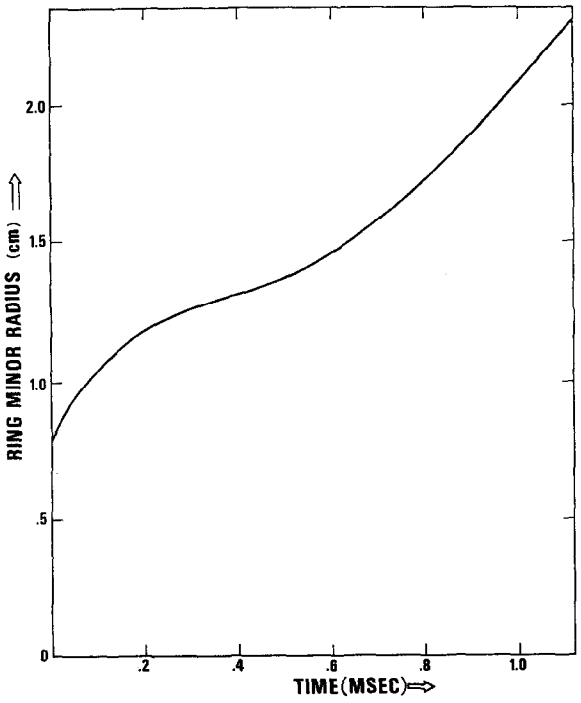

FIG. 4. Ring minor radius versus t.

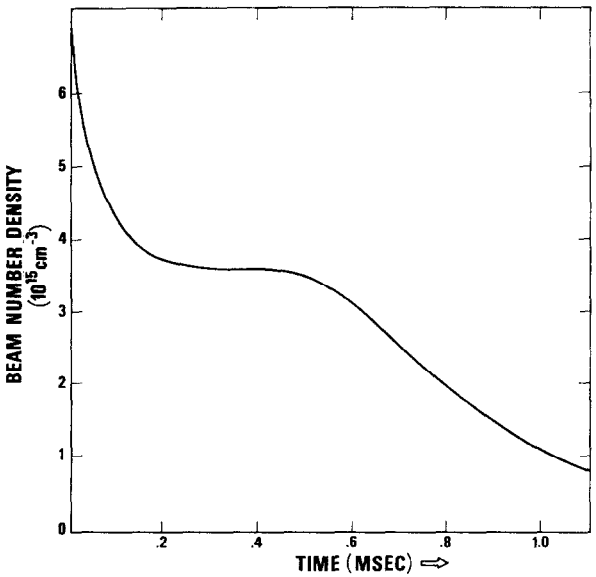

FIG. 5. Beam number density versus t.

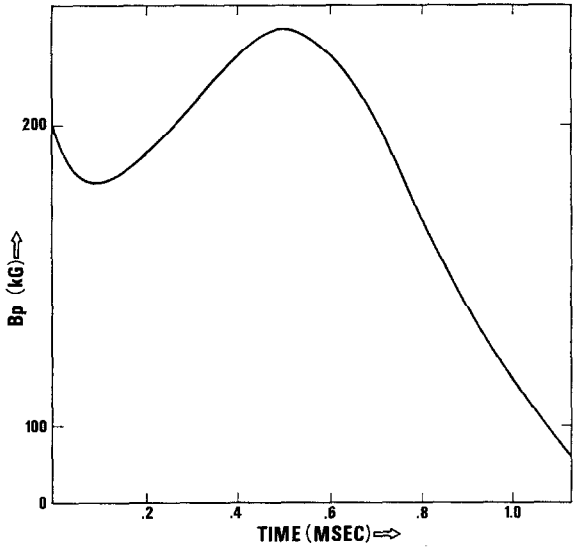

FIG. 6. Poloidal magnetic field versus t.

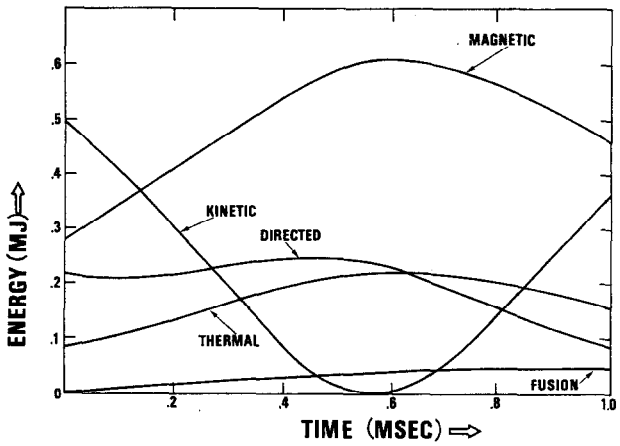

FIG. 7. Magnetic energy [from Eq. (9)], liner kinetic energy, ion streaming energy, and total particle thermal energy versus t.

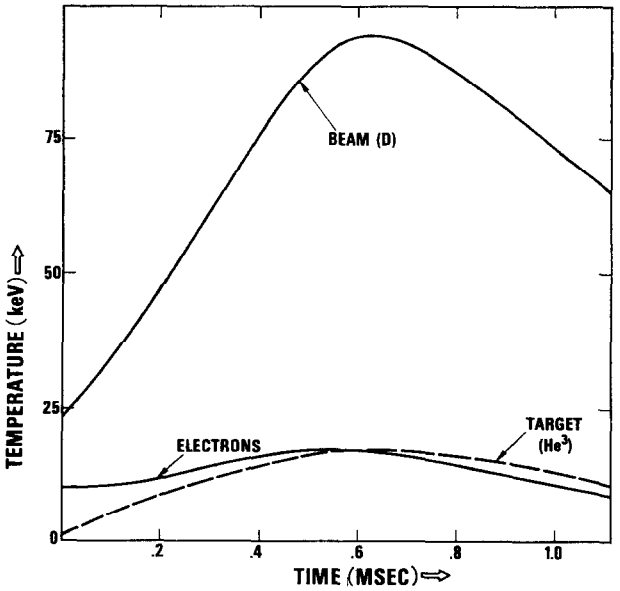

FIG. 8. Beam, target ion, and electron temperatures versus t.

Figure 3 shows how the beam and liner radii change in time. Note that the separation increases, a reflection of the increase in beam minor radius (Fig. 4). Correspondingly, the number densities (Fig. 5) drop, level off as collisional heating and compression come into balance, then drop again in the expansion (decompression) stage, and the poloidal field (Fig. 6) decreases, increases, then decreases monotonically

after turnaround. The various forms of energy (magnetic, liner kinetic, ion directed, and thermal) are plotted in Fig. 7, along with the fusion yield. Figure 8 shows how the component temperatures increase near turnaround, the evident irreversibility being a consequence of collisions.

Running time on the calculation using an IBM 360/168 was 91 s, of which about one quarter was required for diagnostics. Using ten current loops to represent the liner current profile approximately doubles the running time, since roughly twice as many differential equations have to be solved. It turns out to be convenient in writing the code to make extensive use of nested sequences of statement functions in redetermining force balance on each time step, and most of the running time is expended in this task. The number of terms in the flux equation (2) and in the force equation (8) goes as J_{tot}^2 ($J_{\text{tot}} = J_l + 1$ is the present instance) is the total number of current loops. For the examples cited, matrix inversion of Eq. (2) and evaluation of Eq. (8) do not contribute substantially to the running time. An operation count shows that this will continue to be the case until $J_{\text{tot}} \sim 50$. For J_{tot} much larger than this, the penalty for using pairwise forces (instead of solving for the potentials) becomes prohibitive, thus imposing a limitation in principle on the method. As noted in the Introduction, however, the use of large numbers of simulation loops runs counter to the philosophy on which this method is based.

A variety of prescriptions are possible for defining the initial conditions. The main thing is to ensure that they be neither overdetermined nor underdetermined. When working with multiple liner current loops, we arbitrarily imposed the condition that the flux threading all the loops be the same. Though straightforward, this is unlikely to be a good approximation in the late stages of the implosion if finite resistivity is modeled.

VII. Conclusions

We have presented a new numerical technique for solving problems involving the dynamics of charged-particle rings. Its principle advantage is that it is couched in circuit-theoretical terms, obviating the need for solution of partial differential equations. Because of its adaptation to the physics and geometry of such problems, the method can be implemented with only a small number ($\sim$10) of current-carrying elements. In effect, it replaces the uniform or quasi-uniform mesh of the standard two-dimensional finite-difference technique with a highly nonuniform "mesh" of circuit elements, located optimally to reflect the relevant physics.

The code has been applied to calculations of the thermonuclear yield and other characteristics of a beam–target fusion device. The particular concept for which the code was originally developed turns out to be disappointing in terms of its efficiency as a reactor (the example of Section VI yielded $Q \approx 3.2\%$), and also appears to be unstable to kink modes [9]; however it may have nonfusion applications. It is clear that the code can be applied to a variety of axisymmetric situations involving field reversal and changes of system geometry, and therefore is potentially of wider utility.

Recently it has been proposed to increase the intensity of the neutral beams used to heat the plasma in 2 xIIB and similar mirror devices in order to produce field reversal [10]. As pointed out by Baldwin and Rensink [11], electric fields induced by the buildup of current tend to partially cancel the ion current. It is thus unclear that an initially unreversed configuration can become reversed, no matter how much ion current is added. Even if the configuration is compressed radially (by the action, e.g,. of external coils, an imploding liner, or axial translation in a tank with converging metal walls), field reversal is problematic. The flux linking the ion ring tends to be conserved, and collisional diffusion only flattens the profiles.

ACKNOWLEDGMENT

This work was supported by the Office of Naval Research.

REFERENCES

1. P. DREIKE, R. L. FERCH, A. FRIEDMAN, S. HUMPHRIES, R. V. LOVELACE, G. LUDWIG, R. N. SUDAN, D. L. BOOK, G. COOPERSTEIN, A. T. DROBOT, J. GOLDEN, S. A. GOLDSTEIN, C. A. KAPETANAKOS, R. LEE, W. MANHEIMER, S. J. MARSH, D. MOSHER, E. OTT, S. S. STEPHANAKIS, AND P. J. TURCHI, "Plasma Physics and Controlled Nuclear Fusion Research 1976," Vol. 3, p. 415, International At. Energy Agency, Vienna, 1977.
2. S. J. MARSH, A. T. DROBOT, J. GOLDEN, AND C. A. KAPETANAKOS, *Phys. Rev. Lett.* **39** (1977), 705.
3. R. N. SUDAN AND E. OTT, *Phys. Rev. Lett.* **33** (1974), 355.
4. T. OHKAWA, *Nuclear Fusion* **10** (1970), 185.
5. D. L. BOOK AND P. J. TURCHI, *Bull. Amer. Phys. Soc.* **20** (1975), 1278.
6. E. S. WEIBEL, *Phys. Fluids* **20** (1977), 1195.
7. S. I. BRAGINSKII, "Reviews of Plasma Physics," Vol. 1, p. 205, consultants Bureau, New York, 1975.
8. J. M. DAWSON, H. P. FURTH, AND F. H. TENNEY, *Phys. Rev. Lett.* **26** (1971), 1156.
9. R. N. SUDAN AND M. N. ROSENBLUTH, *Phys. Rev. Lett.* **36** (1976), 972; R. N. SUDAN AND M. N. ROSENBLUTH, *Phys. Fluids* **22** (1979), 282.
10. D. E. BALDWIN AND T. K. FOWLER, Lawrence Livermore Laboratory Rept. UCID-17691, 1977.
11. D. E. BALDWIN AND M. E. RENSINK, *Comment. Plasma Phys. Contr. Fusion* **4** (1978), 55.